

Discretization of the Joule heating term for plasma discharge fluid models in unstructured meshes

T. Deconinck, S. Mahadevan, L.L. Raja *

Dept. of Aerospace Engineering and Engineering Mechanics, The University of Texas at Austin, Austin, TX 78712, USA

ARTICLE INFO

Article history:

Received 11 July 2008

Received in revised form 22 January 2009

Accepted 11 March 2009

Available online 20 March 2009

Keywords:

Discharge modeling

Plasma modeling

Numerical method

Joule heating

Unstructured meshes

ABSTRACT

The fluid (continuum) approach is commonly used for simulation of plasma phenomena in electrical discharges at moderate to high pressures (>10's mTorr). The description comprises governing equations for charged and neutral species transport and energy equations for electrons and the heavy species, coupled to equations for the electromagnetic fields. The coupling of energy from the electrostatic field to the plasma species is modeled by the Joule heating term which appears in the electron and heavy species (ion) energy equations. Proper numerical discretization of this term is necessary for accurate description of discharge energetics; however, discretization of this term poses a special problem in the case of unstructured meshes owing to the arbitrary orientation of the faces enclosing each cell. We propose a method for the numerical discretization of the Joule heating term using a cell-centered finite volume approach on unstructured meshes with closed convex cells. The Joule heating term is computed by evaluating both the electric field and the species flux at the cell center. The dot product of these two vector quantities is computed to obtain the Joule heating source term. We compare two methods to evaluate the species flux at the cell center. One is based on reconstructing the fluxes at the cell centers from the fluxes at the face centers. The other recomputes the flux at the cell center using the common drift-diffusion approximation. The reconstructed flux scheme is the most stable method and yields reasonably accurate results on coarse meshes.

© 2009 Elsevier Inc. All rights reserved.

1. Introduction

Fluid (continuum) models have been used since the 1960s to simulate plasma discharge phenomena. Fluid models describe the transport of electrons, ions and neutral species using moments of the species Boltzmann equation coupled to electromagnetic field equations. These models provide spatial and temporal information on averaged properties such as species density and species temperature in discharges and the electromagnetic fields in the discharge. A wide variety of plasmas such as low-pressure glow discharges [1–3], radio-frequency plasma discharges [4–6], dielectric barrier discharges [7], microdischarges [8–11] and streamers [12] have been simulated using the fluid modeling framework.

A typical fluid model solves the following governing equations. The species continuity equation determines the individual species number densities (n_k) in the discharge as follows

$$\frac{\partial n_k}{\partial t} + \vec{\nabla} \cdot \vec{\Gamma}_k = \dot{G}_k, \quad (1)$$

* Corresponding author.

E-mail address: lraja@mail.utexas.edu (L.L. Raja).

where, k represents the species index, $\vec{\Gamma}_k$ is the species drift-diffusion flux, and \dot{G}_k is the gas-phase species generation rate through plasma chemical reactions. The self-consistent electric potential is determined using the electrostatic Poisson's equation

$$\nabla^2 \phi + \frac{e}{\epsilon_0} \sum_{k=1}^{K_g} Z_k n_k = 0, \quad (2)$$

where, ϕ is the potential, e is the unit electric charge, ϵ_0 is the permittivity of free space, K_g is the total number of gas species, and Z_k is the charge number of species k (e.g. -1 for electrons). Electron transport coefficients and the rate coefficients of electron impact reactions are a strong function of the electron energy distribution function which may be parameterized by a local electron temperature (T_e) [8–11]. In case the local fluid approximation is not used, fluid models include an electron energy equation to determine the electron energy density ($e_e = \frac{3}{2} k_B T_e n_e$) in the discharge

$$\frac{\partial e_e}{\partial t} + \vec{\nabla} \cdot \left(\frac{5\vec{\Gamma}_e e_e}{3n_e} \right) - \vec{\nabla} \cdot (\eta_e \vec{\nabla} T_e) = -e\vec{E} \cdot \vec{\Gamma}_e - \frac{3}{2} k_B n_e \frac{2m_e}{m_{k_b}} (T_e - T_g) \bar{\nu}_{e,k_b} - e \sum_{j=1}^{I_g} \Delta E_j^e r_j, \quad (3)$$

where, η_e is the thermal conductivity of electrons, k_B is the Boltzmann's constant, m_e and m_{k_b} are the particle mass of electron and dominant background gas species, respectively, $\bar{\nu}_{e,k_b}$ is the electron momentum transfer collision frequency with the background gas, ΔE_j^e is the energy lost per electron (in eV units) in an inelastic collision event represented by a gas-phase reaction j , r_j is the rate of progress of a reaction j (in $\text{m}^{-3} \text{s}^{-1}$ units), and I_g is the total number of gas-phase reactions. The electrostatic field is determined from the electrostatic potential as $\vec{E} = -\vec{\nabla} \phi$. Finally, the gas temperature (T_g) can be determined through the gas energy equation

$$\frac{\partial}{\partial t} \sum_h n_k h_{k,sens} + \vec{\nabla} \cdot \sum_h \vec{\Gamma}_k h_{k,sens} - \vec{\nabla} \cdot \left(\sum_h \eta_k \vec{\nabla} T_g \right) = -e \sum_h Z_k \vec{\Gamma}_k \vec{E} + \frac{3}{2} k_B n_e \frac{2m_e}{m_{k_b}} (T_e - T_g) \bar{\nu}_{e,k_b} - e \sum_{j=1}^{I_g} \Delta E_j^g r_j, \quad (4)$$

where, $h_{k,sens}$ is the sensible enthalpy of species k , η_k is the thermal conductivity of species k , ΔE_j^g is the energy lost from the thermal pool in an inelastic collision event represented by a gas reaction j , and the index h indicates the summation over all the heavy species. The above gas energy equation uses the constant pressure assumption and neglects fluid mechanical viscous dissipation.

The Joule heating source term, i.e. the first term on the RHS of (3) and (4), constitutes the main source term in the electron energy balance and often times for the gas energy equation. Since reaction rates due to electron impact are exponential functions of the electron temperature, small deviations in the electron energy density can result in significant changes in the predicted discharge characteristics. Most reaction rates also depend on the number density of the background gas, and therefore on the gas temperature. The accuracy of the method used to compute the Joule heating term in the energy balance equations is therefore critical. As shown in [13], the stability of the numerical scheme also depends on the technique used to compute the source term of the electron energy equation owing to temporal stiffness introduced by this term for several types of plasma discharge problems.

Complex two-dimensional or three-dimensional geometries are now commonly encountered in the modeling of plasma discharges. Local mesh refinement is often needed to capture the steep gradients in the number density and in the electric field profiles. To optimize mesh resolution, adaptive mesh techniques can be pursued [12]. For these reasons, the use of unstructured meshes is necessary, as it already is the case for computational fluid dynamics. Robust and accurate numerical methods to simulate gas discharges on unstructured meshes must therefore be developed. Several issues specific to the self-consistent simulations of plasma phenomena using a cell-centered finite-volume approach arise in the context of unstructured meshes, the treatment of the Joule heating term being one. Here we discuss a simple and accurate approach for the numerical treatment of this term in the context of a cell-centered finite-volume discretization of the plasma discharge governing equations on generalized unstructured meshes. The technique can be used on structured meshes as well, where it reduces to a simplified numerical stencil.

2. Numerical method

The governing equations (1)–(4) can be cast in an integral form, by integrating over an arbitrary control volume V as

$$\int_V \frac{\partial \alpha}{\partial t} dV + \int_{\partial V} \vec{\Gamma}_\alpha \cdot d\vec{S} = \int_V S_\alpha dV, \quad (5)$$

where, α is the dependent variable (the species number densities n_k , the electrostatic potential ϕ , the electron energy densities e_e , or the gas temperature T_g), $\vec{\Gamma}_\alpha$ are the fluxes, and S_α are the source terms. In the cell-centered finite-volume scheme for a fixed non-moving mesh, the following spatial discretization is used to approximate (5)

$$V_{\text{cell}} \frac{\partial \alpha_{cc}}{\partial t} + \sum_f \Gamma_{\alpha,fc} A_f = V_{\text{cell}} S_{\alpha,cc}, \quad (6)$$

where, V_{cell} is the cell volume, the index f indicates the summation over all the faces enclosing the cell, A_f is the area of face f , the subscript cc indicates cell-centered value of the corresponding variable, and the subscript fc indicates face-centered values. For the gas discharge governing equations, the fluxes $\Gamma_{\alpha,fc}$ are the normal projections of the species fluxes, the electric field, and the electron and gas energy fluxes at the face centers and are assumed positive directed out of the cell. Figs. 1 and 2, show the locations at which the normal projections of the fluxes are evaluated for a structured and unstructured mesh, respectively.

Several discretization schemes of the fluxes at the face centers are tested in this study. The consistency and accuracy of the following three methods will be shown:

- Central-difference flux:

$$\Gamma_{\alpha,fc} = V_{fc} \left(\frac{\alpha_{cc,1} + \alpha_{cc,2}}{2} \right) - D_{fc} \left(\frac{\alpha_{cc,1} - \alpha_{cc,2}}{\delta} \right). \tag{7}$$

- Upwinded flux:

$$\begin{aligned} \Gamma_{\alpha,fc} &= V_{fc} \alpha_{cc,1} - D_{fc} \left(\frac{\alpha_{cc,1} - \alpha_{cc,2}}{\delta} \right) \quad \text{if } V_{fc} > 0, \\ \Gamma_{\alpha,fc} &= V_{fc} \alpha_{cc,2} - D_{fc} \left(\frac{\alpha_{cc,1} - \alpha_{cc,2}}{\delta} \right) \quad \text{if } V_{fc} < 0. \end{aligned} \tag{8}$$

- Scharfetter–Gummel Flux [14]:

$$\begin{aligned} \Gamma_{\alpha,fc} &= V_{fc} \left(\alpha_{cc,1} + \frac{\alpha_{cc,1} - \alpha_{cc,2}}{\exp(Pe) - 1} \right), \quad \text{if } Pe = \frac{V_{fc} \delta}{D_{fc}} > 0, \\ \Gamma_{\alpha,fc} &= V_{fc} \left(\alpha_{cc,2} + \frac{\alpha_{cc,1} - \alpha_{cc,2}}{\exp(-Pe) - 1} \right), \quad \text{if } Pe = \frac{V_{fc} \delta}{D_{fc}} < 0. \end{aligned} \tag{9}$$

where V_{fc} is the convective velocity at the face center (e.g. $-\mu_e E_{fc}$ for the electron flux), $\alpha_{cc,1}$ and $\alpha_{cc,2}$ are the solution variables at the two neighboring cell centers, and D_{fc} is the diffusion coefficient at the face center. The convective velocity and the flux are assumed positive directed from the first cell towards the second cell. The solution variable (α) in the transport term is handled implicitly to allow time step sizes that exceed the CFL (Courant-Fredrich-Lewy) limitation [13].

The cell-centered value of the Joule heating source term contribution to $S_{z,cc}$, appearing in both (3) and (4), can be evaluated by first evaluating the contribution at the face centers (where the fluxes are available), and then interpolating the Joule heating source term at the cell center. This technique has been used by several authors on structured meshes [6,10,13]. Using this approach, the Joule heating is evaluated as follows for a two-dimensional structured mesh (see Fig. 1)

$$\begin{aligned} [\vec{E} \cdot \vec{\Gamma}](i,j) &= \frac{1}{2} [E_x(i+1/2,j)\Gamma_x(i+1/2,j) + E_x(i-1/2,j)\Gamma_x(i-1/2,j) + E_y(i,j+1/2)\Gamma_y(i,j+1/2) \\ &+ E_y(i,j-1/2)\Gamma_y(i,j-1/2)]. \end{aligned} \tag{10}$$

In (10) the subscript k is dropped from the species flux term $\vec{\Gamma}_k$ for convenience. The subscripts x and y refers to the coordinate directions and the symbols i and j , refer to the node locations in a structured mesh (Fig. 1). The Joule heating in (10) is computed by adding the average contribution of the dot product in the x and y directions. Note that it is not simply an average of the product $\vec{E} \cdot \vec{\Gamma}$ computed on each face, in which case the factor in the denominator would have been 4 instead of 2. The reason this method can be used on structured meshes is because the face normals lie exactly along the coordinate

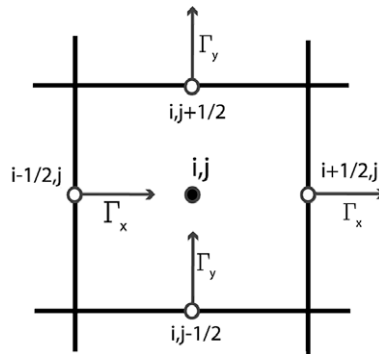


Fig. 1. Orthogonal two-dimensional structured mesh. Scalar solution variables are evaluated at the cell center (point with solid circle). The x - and y -components of the fluxes are evaluated at the face centers (points with open circles).

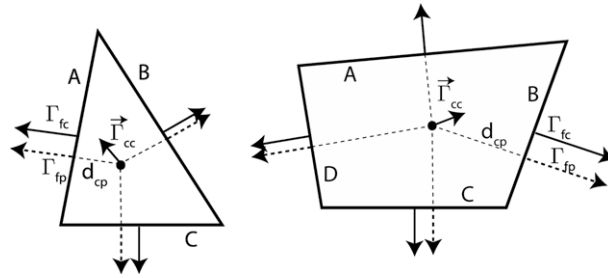


Fig. 2. Reconstruction of the species flux at the cell center (for a triangular and quadrilateral cell) based on the normal projection of the fluxes at the face centers. The dotted lines are perpendiculars to the faces that intersect the cell center.

directions. On an unstructured mesh, the face normal orientation is arbitrary and hence an extension of (10) is not straightforward.

We propose the following approach to computing the Joule heating source term on a general unstructured mesh with closed convex cells. The term is computed directly at the cell centers by evaluating the dot product of the electric field and the species flux at the cell centers. The two vector quantities can be evaluated explicitly at the cell centers (\vec{E}_{cc} and $\vec{\Gamma}_{cc}$, respectively) using solution variables and fluxes already computed at the faces for the Poisson’s (2) and species continuity equations (1) by the cell-centered finite-volume method. The face fluxes are nominally available at the face centers (fc). The Green-Gauss or least-squares reconstruction [15] techniques are commonly used to evaluate the gradient of cell-centered solution variables. Because of ease of implementation, we chose to use the Green-Gauss method to obtain the electric field from the potential field. By this method, the gradient is constructed by applying the Green-Gauss theorem to individual cell volumes in the mesh as follows,

$$(\vec{\nabla}\phi)_{cc} = \frac{1}{V_{cell}} \sum_f \phi_{fc} \vec{A}_f, \tag{11}$$

where, ϕ_{fc} is the value of potential at the face center, \vec{A}_f is the normal area vector of face f (pointing away from the cell), and the summation is over all the faces enclosing the cell. One can interpolate the face-centered value ϕ_{fc} from the values of the potential at the two neighboring cells centers using a simple average or a higher-order weighted averaging procedure.

Evaluation of the species flux vector value at the cell center ($\vec{\Gamma}_{cc}$) however poses a special problem since only the normal projection of the species fluxes (Γ_{fc}) are available at the face centers through the cell-centered finite-volume method. We propose to reconstruct the species flux vector at the cell center from these normal projections of the species fluxes at the faces enclosing the cell. We refer to this approach as the “Reconstruction-Flux” scheme which we depict in Fig. 2. To first-order, we assume that the flux we are reconstructing ($\vec{\Gamma}$) is piecewise constant within each cell. This implies that the flux field is irrotational within each cell and that there exists a scalar, ψ , such that $\vec{\Gamma} = \vec{\nabla}\psi$. We assign an arbitrary constant value K to ψ at the cell center. At each face enclosing the cell, we define a new point fp , such that the face area normal vector through the point fp is collinear with cell center cc . If the normal projection of the species flux at fc (Γ_{fc}) is assumed a constant across the entire face, the normal projection of the species flux at the point fp (Γ_{fp}) is equal to Γ_{fc} . We can now estimate the value of ψ at fp (ψ_{fp}) for each face by performing a line integration along the line joining cc and fp , i.e.

$$\psi_{fp} = K + d_{cp} \Gamma_{fp}, \tag{12}$$

where, d_{cp} is the distance between cc and fp .

Finally, the Green-Gauss theorem is used to compute the “Reconstruction-Flux” at the cell center

$$\vec{\Gamma}_{cc} = \frac{1}{V_{cell}} \sum_f \psi_{fc} \vec{A}_f. \tag{13}$$

Here the value of ψ_{fc} can be approximated as being equal to ψ_{fp} . Expanding the summation in (13), we obtain

$$\vec{\Gamma}_{cc} = \frac{1}{V_{cell}} \sum_f (K + d_{cp} \Gamma_{fp}) \vec{A}_f = \frac{1}{V_{cell}} \sum_f (d_{cp} \Gamma_{fp}) \vec{A}_f. \tag{14}$$

In (14), the term $\sum_f K \vec{A}_f = (K \sum_f \vec{A}_f)$ equals 0 for all closed cells. The above formulation reconstructs the cell center value of the species flux vector based on known normal projections of the species fluxes at the faces and other mesh information only.

For an orthogonal structured mesh (as shown in Fig. 1), the “Reconstruction-Flux” scheme reduces to

$$[\vec{E} \cdot \vec{\Gamma}](i,j) = \frac{[E_x(i+1/2,j) + E_x(i-1/2,j)]}{2} \frac{[\Gamma_x(i+1/2,j) + \Gamma_x(i-1/2,j)]}{2} + \frac{[E_y(i,j+1/2) + E_y(i,j-1/2)]}{2} \times \frac{[\Gamma_y(i,j+1/2) + \Gamma_y(i,j-1/2)]}{2}. \tag{15}$$

In (15), the electric field and species flux are evaluated at the cell center before performing their dot product, while in (10) the Joule heating is evaluated at the face centers and then interpolated at the cell center.

As an alternative to the above approach, one could also choose to recompute the species flux at the cell center with the same drift-diffusion approximation that is used to compute the flux at the face centers

$$\vec{\Gamma}_k = -\mu_k n_k \vec{\nabla} \phi - D_k \vec{\nabla} n_k, \quad (16)$$

where μ_k and D_k are the mobility and diffusion coefficients of species k . We will call this method the “Recomputed-Flux” scheme. The number density (n_k) is already available at the cell center and the electric field and gradient of the species number density can be evaluated by the Green-Gauss method (13). In most models [9–11], electron fluxes at the face centers are discretized with the Scharfetter–Gummel exponential scheme to overcome the stiffness in the drift-diffusion form of the electron flux. This approach to evaluating the electron fluxes at the cell center (with reconstruction gradients) is therefore not consistent with the electron fluxes evaluated at the face centers (with the exponential scheme). Consequences of this inconsistency will be discussed in the next section.

3. Results

3.1. Test case

We consider a one-dimensional direct-current glow discharge between two infinitely large planar electrodes. The inter-electrode distance is 1 cm and the pressure is 1 Torr. A constant voltage difference of 250 V is applied between the two electrodes. The pure argon discharge gas is considered with the argon plasma modeled by three species (ground state atoms Ar , ions Ar^+ and electrons e^-). The species continuity equation is solved for the ions and the electrons, while the background argon number density is held constant. For computational expediency, we assume a simplified chemistry comprising a single ionization reaction due to electron impact ($e + Ar \rightarrow 2e + Ar^+$). An independent solution of the zero-dimensional electron Boltzmann equation (using the BOLSIG+ software [16]) provides the reaction rate coefficient and the electron transport coefficients as function of the electron temperature. The ion transport properties are derived from experimental mobility data [17]. A constant value of the secondary emission coefficient of 0.05 is assumed for the ions impacting at the surface which produce a flux of electrons entering the discharge depending on the ion flux leaving the discharge to wall surfaces. We test our numerical method for computing the Joule heating term in the electron energy equation alone. The gas energy equation is not solved and a constant gas temperature of 300 K is assumed. The boundary conditions employed in this study are similar to the ones described in detail in Ref. [10]. Kinetically limited flux conditions are used for the flux of electrons at the solid surfaces, while mobility limited flux conditions are imposed for all ions at the surfaces. Dirichlet boundary conditions with specified potentials are used for the Poisson’s equation. The simulations are typically started with uniform initial conditions for the field variables; e.g. zero potential, an electron temperature of 10,000 K, and charged species densities of 10^{14} m^{-3} for the electrons and ions such that the plasma is quasineutral.

Figs. 3 and 4 show mesh-converged results for which the “Reconstruction-Flux” scheme has been used using a 1000-cell mesh as discussed below. The cathode is placed at $x = 0$ cm and the anode at $x = 1$ cm. A peak number density of ionized species of $\sim 10^{16} \text{ \#/m}^3$ is observed in the quasineutral region of the plasma. The cathode sheath occupies $\sim 25\%$ of the dis-

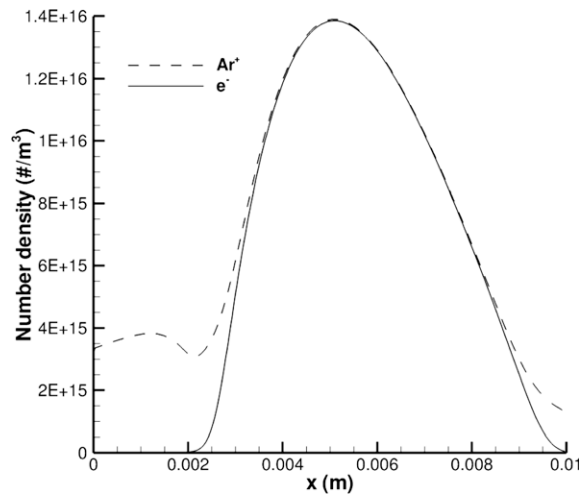


Fig. 3. Charged species number density profile for a one-dimensional 250-V Argon discharge (1 Torr) obtained using a 1000-cell mesh that satisfies mesh-convergence on all of the numerical methods used.

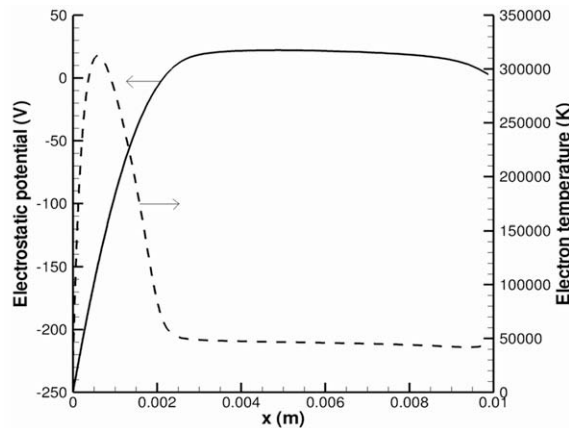


Fig. 4. Electrostatic potential and electron temperature profiles for a one-dimensional 250-V Argon discharge (1 Torr) obtained using a 1000-cell mesh that satisfies mesh-convergence on all of the numerical methods used.

charge. A sharply peaked electron production profile (not shown) is located at the sheath edge. The electron temperature is ~ 4 eV in the bulk plasma and increases to ~ 20 eV in the cathode sheath. The current density for these conditions is ~ 0.2 mA/cm². Results obtained with different schemes will be compared next. We use the computed value of the current density as a metric for comparing the accuracy between the different numerical methods. The peak number density of the ionized species (Ar^+) has also been used and yields the same results.

3.2. One-dimensional mesh

We first discuss results for the above test case using a one-dimensional version of the self-consistent plasma model, where solution variables vary only in the direction perpendicular to the inter-electrode plane. Since a two-dimensional implementation of the above method is used, the numerical solution to this one-dimensional problem is enabled by stacking a layer of single quadrilateral cells and imposing zero-flux boundary conditions in the other directions. The numerical schemes discussed above have been tested on three different meshes: a 60-cell, 250-cell and 1000-cell mesh. These meshes are stretched to obtain a better resolution of the cathode sheath region. Note that most two-dimensional simulations of gas discharges presented in the literature do not use more than ~ 50 mesh points in the electric field direction (inter-electrode direction) to capture the cathode sheath of glow discharges. The coarsest mesh discussed in this paper is therefore representative of a majority of the modeling work reported in the literature. The three flux discretization schemes, together with the “Reconstruction-Flux” discretization for the Joule heating source term, were stable on the three meshes for time steps smaller than $\sim 10^{-9}$ s. The same discretization scheme was used for all the species fluxes and energy fluxes. Starting from arbitrary initial conditions, a steady state was reached after $\sim 10^{-4}$ s. Fig. 5 shows the computed current density obtained at steady state for the different face flux discretization schemes on the three meshes. Only the exponential scheme provides reasonably accurate results on the coarsest mesh. The central scheme fails to yield accurate results on coarse meshes. Negative values and oscillations appear for the electron density and electron temperature profiles in the cathode sheath region, which pollutes the entire solution. The upwind scheme is the most diffusive, and provides the least accurate solution even on

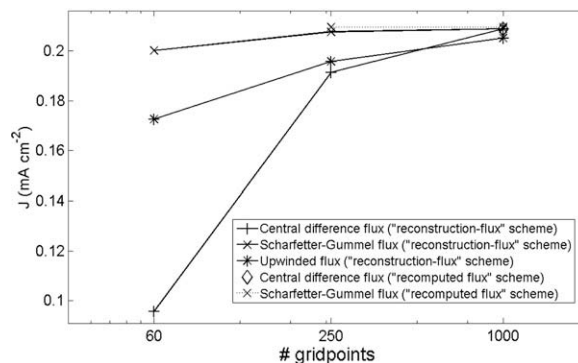


Fig. 5. Computed current densities obtained on one-dimensional meshes with the different numerical schemes (see Fig. 3 caption for physical conditions of the discharge).

the 1000-cell mesh. The good agreement between the solutions from the different schemes on the finest mesh confirms that all the numerical schemes are consistent. The “Reconstruction-Flux” discretization for the Joule heating source term was compared to the approach presented in (10) and both methods yield similar results for the different face flux discretization schemes. The difference in the computed current density was typically less than 1%.

The “Recomputed-Flux” Joule heating term discretization was also tested on the different meshes and with the three face flux discretization schemes. The upwind scheme, combined with the “Recomputed-Flux” discretization, was found to be unstable on the three meshes (for arbitrarily small values of the time step). For time steps smaller than $\sim 10^{-9}$ s, the central-difference scheme is stable only on the 1000-cell mesh, while the exponential scheme is stable on the 250- and 1000-cell mesh. Fig. 5 shows the current density obtained with the “Recomputed-Flux” Joule heating discretization for those cases where a stable solution was obtained. The accuracy of the solutions is comparable with those obtained with the “Reconstruction-Flux” Joule heating term discretization. Fig. 6 shows the electron fluxes at the cell centers computed with the Scharfetter–Gummel exponential discretization scheme on the 250-cell and 1000-cell meshes. The “Recomputed-Flux” Joule heating term discretization fails to accurately estimate the electron flux on coarse meshes. The drift and diffusion components of the electron fluxes are sharply peaked at the cathode sheath and largely cancel each other if evaluated properly. The “Recomputed-Flux” discretization yields a non-monotonic electron flux on coarse meshes, which leads to numerical instabilities and therefore fails to predict discharge phenomena accurately.

3.3. Two-dimensional mesh

The above one-dimensional test case is now simulated using two-dimensional unstructured meshes by applying appropriate zero-flux boundary conditions for all equation in the second direction. Three different unstructured meshes are used to demonstrate our proposed “Reconstruction-Flux” discretization for the Joule heating source term. These two-dimensional meshes are shown in Fig. 7. The length of the three meshes is 1 cm, while their width is 0.4 cm. Mesh (a) in Fig. 7 comprises relatively uniform triangles and is coarser than the triangular mesh (b) which is refined toward the cathode. Mesh (c) contains both triangular and quadrilateral cells and comprises highly skewed cells. The presence of highly skewed cells in mesh (c) therefore leads to high discretization errors and can also affect stability of the numerical schemes. Mesh (a), (b) and (c) comprises 2016, 4972 cells, and 2228 cells respectively. As with the one-dimensional meshes, the three face flux discretization schemes, together with the “Reconstruction-Flux” Joule heating discretization, are stable for time steps smaller than $\sim 10^{-9}$ s. Table 1 shows the current density obtained with the different numerical schemes. For comparison, the mesh-converged current density (obtained with the central-difference scheme or Scharfetter–Gummel scheme on the 1000-cell one-dimensional mesh) was 0.209 mA cm^{-2} . The central-difference discretization scheme is the most accurate method on the triangular meshes while the solution obtained with the Scharfetter–Gummel scheme is reasonably accurate. No oscillations or negative values of the electron temperature or electron density are observed on the two-dimensional triangular meshes. On the mesh (c) with highly skewed cells, the exponential scheme yields the most accurate results (small oscillations appears the for central-difference scheme). The solution obtained with the upwind discretization scheme is quite diffusive on all meshes. Fig. 7 shows the electron temperature profiles obtained with the exponential scheme. The nonuniformities that appear in the transverse direction (direction parallel to electrode plane) on mesh (c) clearly show the limitations of our first-order model for highly skewed cells.

The “Recomputed-Flux” Joule heating term discretization combined with the upwind or Scharfetter–Gummel exponential face flux discretization scheme is unstable on all the unstructured meshes (regardless of the value of the time step). Only the central-difference scheme is stable with this method for the two triangular unstructured meshes. This confirms that the

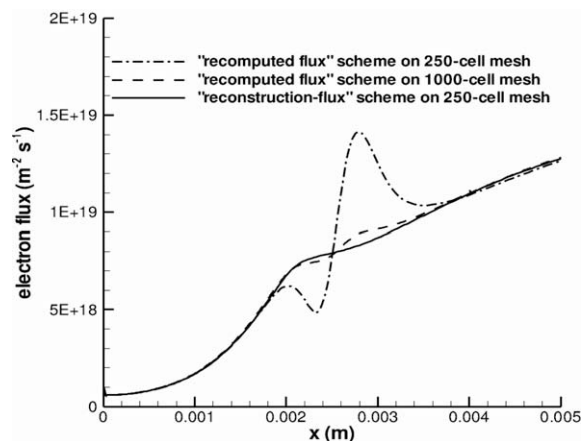


Fig. 6. Computed electron fluxes on one-dimensional meshes with different numerical schemes (see Fig. 3 caption for conditions of the discharge). The figure shows a close-up of the solution in the cathode sheath region.

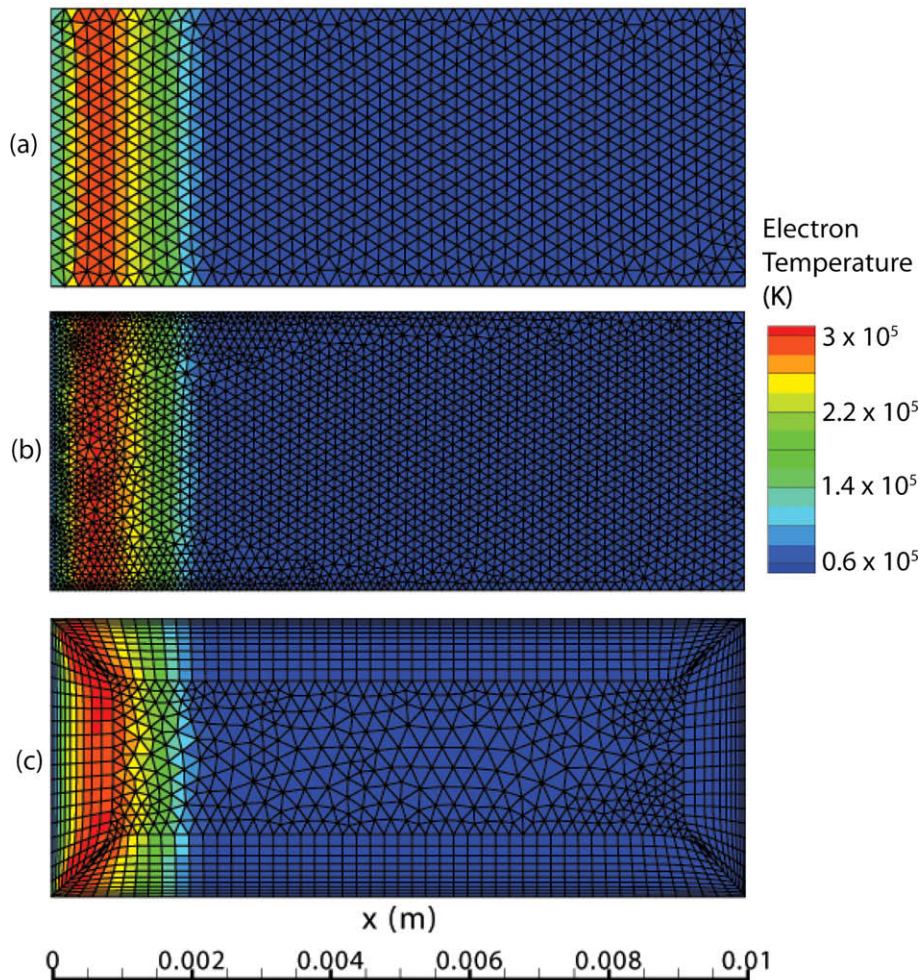


Fig. 7. Computed electron temperature profiles obtained with the “Reconstruction-Flux” method (combined with the exponential discretization of the fluxes) on two-dimensional unstructured meshes (see Fig. 3 caption for the conditions of the discharge).

Table 1

Computed current densities (in mA cm^{-2}) obtained on the two-dimensional meshes with the different numerical schemes (see Fig. 3 caption for conditions). The mesh-converged current density (obtained with the central-difference scheme on the 1000-cell one-dimensional mesh) is 0.209 mA cm^{-2} . Crosses indicate that a stable solution could not be obtained due to numerical instabilities.

	“Reconstruction-Flux” scheme			“Recomputed-Flux” scheme		
	Upwind	Central	S-G	Upwind	Central	S-G
Coarse triangular mesh (a)	0.167	0.198	0.193	x	0.181	x
Refined triangular mesh (b)	0.184	0.208	0.205	x	0.205	x
Mixed triangles and quadrilaterals with skewed cells mesh (c)	0.166	0.225	0.211	x	x	x

“Recomputed-Flux” discretization is less robust than the “Reconstruction-Flux” discretization approach. As shown in Table 1, the results obtained with the “Recomputed-Flux” discretization are also less accurate than those obtained with the “Reconstruction-Flux” discretization.

4. Conclusion

An effective approach to numerical discretization of the Joule heating source term for fluid models of plasma discharge phenomena is presented in this paper. The method, which we call the “Reconstruction-Flux” discretization, has been developed for a cell-centered finite-volume scheme of the gas discharge governing equations on unstructured meshes. In this

method, the Joule heating term is computed by evaluating the dot product of the electric field and the species flux at the cell center. The species flux at the cell center is reconstructed based on the normal projection of the species fluxes at the faces enclosing the cell. The method was validated by simulating a one-dimensional argon glow discharge on different meshes. We compared the “Reconstruction-Flux” discretization of the Joule heating source term with another method where the flux is recomputed at the cell center with the drift-diffusion approximation. The “Reconstruction-Flux” discretization approach is found to be a robust and accurate method on structured and unstructured meshes. This method, combined with the Scharfetter–Gummel exponential face flux discretization scheme, produces reasonably accurate results even on coarse meshes.

References

- [1] J.-P. Boeuf, A two-dimensional model of dc glow discharges, *J. Appl. Phys.* 63 (1988) 1342.
- [2] S.T. Surzhikov, J.S. Shang, Two-component plasma model for two-dimensional glow discharges in magnetic field, *J. Comput. Phys.* 199 (2004) 437.
- [3] S. Mahadevan, L.L. Raja, Simulations of direct-current air surface plasma discharges in supersonic flow, *AIAA Paper 2009-1192*, 47th Aerospace Sciences Meeting, Orlando, Florida, 5–8 Jan 2009.
- [4] G.C. Chen, L.L. Raja, Fluid modeling of electron heating in low-pressure, high-frequency capacitively coupled plasma discharges, *J. Appl. Phys.* 96 (2004) 6073.
- [5] J.-P. Boeuf, Numerical model of rf glow discharges, *Phys. Rev. A* 36 (1987) 2782.
- [6] E.P. Hammond, K. Mahesh, P. Moin, A numerical method to simulate radio-frequency plasma discharges, *J. Comput. Phys.* 176 (2002) 402.
- [7] Y.B. Golubovskii, V.A. Maiorov, J.F. Behnke, J. Tepper, M. Lindmayer, Study of the homogeneous glow-like discharge in nitrogen at atmospheric pressure, *J. Phys. D: Appl. Phys.* 37 (2004) 1346.
- [8] Q. Wang, D.J. Economou, V.M. Donnelly, Simulation of a direct current microplasma discharge in helium at atmospheric pressure, *J. Appl. Phys.* 100 (2006) 023301.
- [9] M.J. Kushner, Modelling of microdischarge devices: plasma and gas dynamics, *J. Appl. Phys.* 38 (2005) 1633.
- [10] P.S. Kothnur, L.L. Raja, Two-dimensional simulation of a direct-current microhollow cathode discharge, *J. Appl. Phys.* 97 (2005) 043305.
- [11] T. Deconinck, L.L. Raja, Modeling of mode transition behavior in argon microhollow cathode discharges, *Plasma Processes and Polymers* 6 (2009).
- [12] A.P. Papadakis, G.E. Georghiou, A.C. Metaxas, New high quality adaptive mesh generator utilized in modeling plasma streamer propagation at atmospheric pressures, *Plasma Source Sci. Technol.* 14 (2005) 250.
- [13] G.J.M. Hagelaar, G.M.W. Kroesen, Speeding up fluid models for gas discharges by implicit treatment of the electron energy source term, *J. Comput. Phys.* 159 (2000) 1.
- [14] D.L. Scharfetter, H.K. Gummel, Large-signal analysis of a silicon read diode oscillator, *IEEE Trans. Electron Devices* ED-16 (1969) 64.
- [15] J.H. Ferziger, M. Peric, *Computational Methods for Fluid Dynamics*, Springer, New York, 1997.
- [16] G.J.M. Hagelaar, L.C. Pitchford, Solving the Boltzmann equation to obtain electron transport coefficients and rate coefficients for fluid models, *Plasma Source Sci. Technol.* 14 (2005) 722.
- [17] H.W. Ellis, R.Y. Pai, E.W. McDaniel, E.A. Mason, L.A. Vielhand, Transport properties of gaseous ions over a wide energy range, *At. Data Nucl. Data Tables* 17 (1976) 177.